JACS JOURNAL OF THE AMERICAN CHEMICAL SOCIETY

Article

pubs.acs.org/JACS

Mechanism for Si–Si Bond Rupture in Single Molecule Junctions

Haixing Li,[†] Nathaniel T. Kim,[‡] Timothy A. Su,[‡] Michael L. Steigerwald,[*,‡] Colin Nuckolls,[*,‡] Pierre Darancet,[*,§] James L. Leighton,[*,‡] and Latha Venkataraman[*,†,‡]

[†]Department of Applied Physics and Applied Mathematics, Columbia University, New York, New York 10027, United States

[‡]Department of Chemistry, Columbia University, New York, New York 10027, United States

[§]Center for Nanoscale Materials, Argonne National Laboratory, Argonne, Illinois 60439, United States

Supporting Information

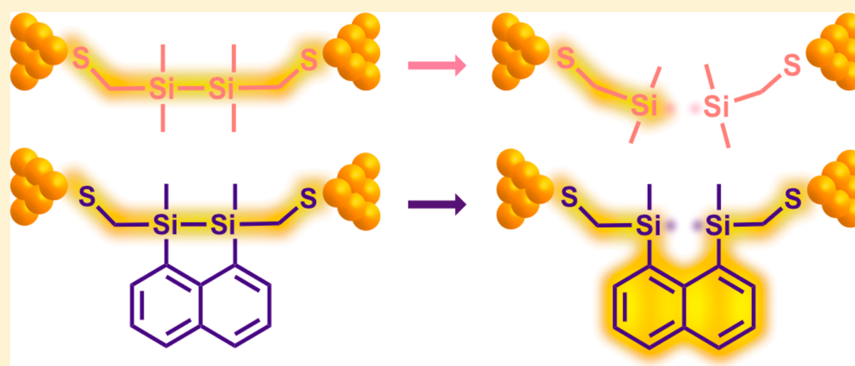

ABSTRACT: The stability of chemical bonds can be studied experimentally by rupturing single molecule junctions under applied voltage. Here, we compare voltage-induced bond rupture in two Si–Si backbones: one has no alternate conductive pathway whereas the other contains an additional naphthyl pathway in parallel to the Si–Si bond. We show that in contrast to the first system, the second can conduct through the naphthyl group when the Si–Si bond is ruptured using an applied voltage. We investigate this voltage induced Si–Si bond rupture by ab initio density functional theory calculations and molecular dynamics simulations that ultimately demonstrate that the excitation of molecular vibrational modes by tunneling electrons leads to homolytic Si–Si bond rupture.

INTRODUCTION

Silicon is a vital component of modern information technology, where it serves as the active material in transistors, integrated circuits, and fiber optics. With an increasing demand for miniaturized electronics, new forms of silicon devices are being investigated including two-dimensional silicene transistors,[1] silicon nanowire transistor[2] and photovoltaic devices,[3−5] nanoscale silicon photonic devices,[6,7] and silicon-based single molecule devices.[8,9] A thorough understanding of the mechanical and electrical characteristics of Si–Si bonds is thus of essential importance as silicon based materials are fast approaching the molecular scale. Here, we focus on the failure mechanism of silicon and investigate voltage-induced rupture of the Si–Si bond in the context of single molecule junctions.

Though individual Si–Si bond strength is only 2.3 eV (for example, C–C bond strength is 3.7 eV with the same valence configuration),[10] networks of Si–Si bonds are ubiquitous in electronic devices. It is therefore crucial to investigate the stability of Si–Si bonds under an applied electric field. Previously, we had measured the electric field breakdown properties of Si–Si bonds; however, we could not rule out bond breakage at other locations along the backbone. In this study, we conclusively demonstrate that bond breakage can occur at the Si–Si bond by devising a double-backbone system. We find that in the double-backbone molecule, conductance occurs through the alternate pathway after the Si–Si bond is broken. We also support our experimental results with computations that suggest strongly that the Si–Si bond ruptures under an applied bias.

We synthesize and study two molecules (**Si2** and **Si2Naph**). **Si2** has a single backbone comprising a Si–Si bond; **Si2Naph** has a double backbone that features a mechanically robust carbon linkage in parallel with the Si–Si bond. We apply a large voltage across the molecular junctions formed with these two molecules and compare their rupture behaviors. We observe different conductance values of the junctions formed with these two molecular backbones when the junctions break, signifying Si–Si bond ruptures in both cases. We attribute this voltage-dependent bond rupture to a current-induced mechanism involving heating of the molecule through electron-vibrational mode coupling. We calculate the molecular vibrational modes using density functional theory and find that a number of modes involving Si–Si bond stretching can be excited since

Received: October 17, 2016
Published: November 18, 2016

ACS Publications © 2016 American Chemical Society

DOI: 10.1021/jacs.6b10700
J. Am. Chem. Soc. 2016, 138, 16159−16164

they are within the applied voltage for both junctions studied. We further carry out molecular dynamics simulations to show that the Si−Si bond is more likely to break upon current-induced heating than the Si−C or Au−S bond, which are also present in the junctions.

■ RESULTS AND DISCUSSION

Synthesis. We prepare **Si2** using previously published methods[11] and naphthyldisilane **Si2Naph** by the sequence shown in Scheme 1.[11−15] The synthesis begins with bis-metalation of 1,8-dibromonaphthalene by lithium halogen exchange and treatment of the resulting dianion with 1,1,2,2-tetrachloro-1,2-dimethyldisilane followed by in situ treatment with the anion formed from bromochloromethane and *n*-BuLi to give **1** in 44% overall yield (Scheme 1). Displacement of the chlorides with KSAc delivered **2** in 62% yield, and reductive cleavage of the acetates provides **Si2Naph** in 93% yield. Compounds **1**, **2**, and **Si2Naph** were all isolated and employed as 1.2:1 mixtures of diastereomers. The trans and cis isomers of both **2** and **Si2Naph** were also separated and characterized (see the SI for details).

Scheme 1. Synthesis of Si2Naph

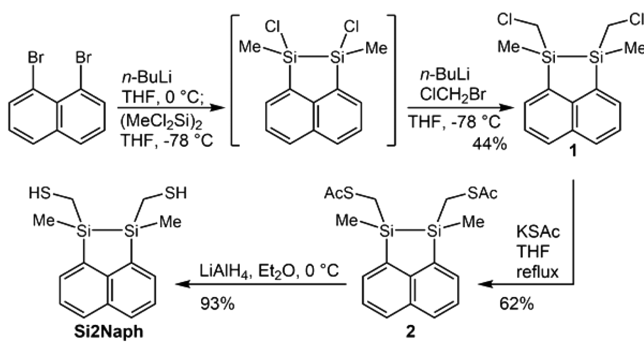

Conductance Measurement. We first measure the conductance of **Si2Naph** and **Si2** (structures are shown in Figure 1a) with the scanning tunneling microscope based break junction technique (STM-BJ) (schematic in Figure 1b).[16,17] In this technique, we repeatedly bring the Au STM tip into and out of contact with the substrate and record the conductance (current/voltage) of the junction as we withdraw the tip. We see plateaus at integer multiples of the conductance quantum ($G_0 = 2e^2/h$) corresponding to atomic Au contact in each conductance-displacement trace. We then see additional features below 1 G_0 once we add a solution of the target molecule in 1,2,4-trichlorobenzene. These features below 1 G_0 signify that an Au−molecule−Au junction is formed after the Au contact breaks. Here we use thiols as the terminal groups to attach the silicon backbone to the Au electrodes by forming Au−S covalent bonds.[11] We collect thousands of traces and compile them into logarithmically binned one-dimensional histograms shown in Figure 1c.

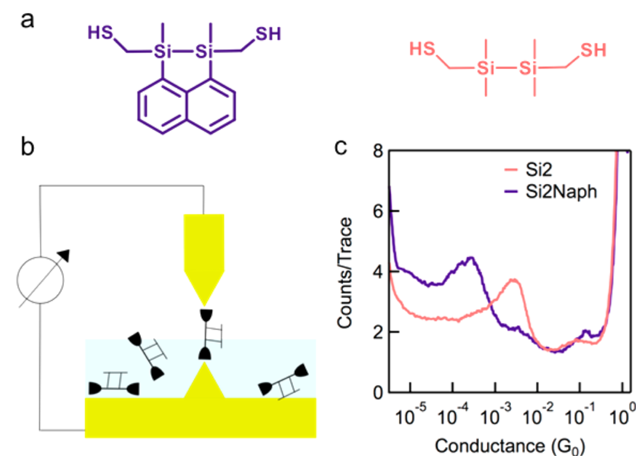

Figure 1. (a) Chemical structures of **Si2Naph** (purple) and **Si2** (pink). (b) Schematic of STM-BJ setup. (c) Logarithmically binned conductance histograms for **Si2Naph** and **Si2** generated without data selection using 100 bins/decade from 17 000 and 27 000 traces, respectively.

We see that **Si2Naph** shows a conductance peak at 2.4×10^{-4} G_0, about one-tenth of the conductance for **Si2**. We note here that the cis and trans isomers of **Si2Naph** show similar results in conductance measurements (SI Figure S1), unlike the analogous molecules terminated with thioanisole linkers,[15] the cis isomer of which, uniquely, forms a high-conducting junction with one of the Au electrodes coupling directly to the Si−Si bond.

Bond Rupture Measurement. Next, we investigate the rupture behaviors of the junctions formed with these two molecules under an applied voltage. We use a modified experimental technique that we have described in detail previously.[11] Briefly, we start with an Au−Au contact and withdraw the tip to a fixed distance to form a single molecule junction. We then hold the junction for 150 ms and withdraw the tip again until the junction breaks by applying a modified ramp to the piezo as shown by the blue trace in Figure 2a. We apply a voltage pulse ranging in amplitude from 0.2 to 1.4 V when the junction is held (green trace in Figure 2a) and record the junction conductance during the entire trace. We first select traces with a conductance within the range of the conductance histogram peak (range indicated by dashed lines in Figure 2b,c) at the start of the hold segment. Of these traces, we observe that some show a roughly constant conductance during the high-bias pulse whereas others show a sudden drop below the molecular conductance range. The former traces (light shades of red/purple for **Si2**/**Si2Naph**) correspond to those with a molecular junction that sustains the high-voltage, while the latter (dark shades of red/purple for **Si2**/**Si2Naph**) are molecular junctions that rupture under the high voltage.

Our primary finding here is that **Si2** junctions break to a conductance that is at our instrument noise floor, whereas the **Si2Naph** junctions break to a conductance that is slightly smaller than that of the **Si2Naph** junction. We analyze all traces that start with a molecular junction and determine the fraction that break under the applied bias using an automated algorithm. Through this analysis, we determine the breaking probabilities for **Si2** and **Si2Naph** molecular junctions based on the measurement of 6000 traces at each applied voltage and plot them in the insets of Figure 2b,c. **Si2** shows a sharp increase at 0.9 V and **Si2Naph** shows a rather linear increase across the whole bias range from 0.2 to 1.4 V.

To investigate further whether the difference in the broken junction conductance between **Si2** and **Si2Naph** is statistically significant, we create separate two-dimensional conductance histograms of all the traces that either sustain or break at an applied bias of 0.9 V. We see in Figure 3a,b that both **Si2** and **Si2Naph** junctions that sustain the high bias display a conductance around their conductance peak values (as seen

DOI: 10.1021/jacs.6b10700
J. Am. Chem. Soc. 2016, 138, 16159−16164

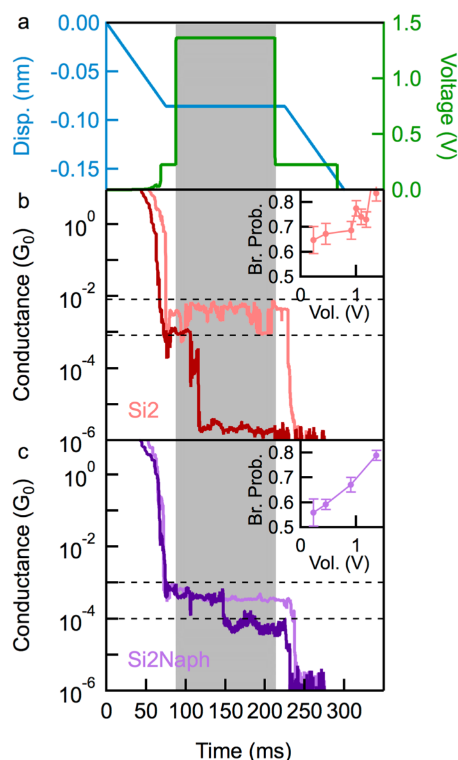

Figure 2. (a) Piezo displacement (blue; left) and applied voltage (green; right) plotted against time in each pull-hold-pull measurement. (b (and c)) Two sample traces measured with **Si2** (**Si2Naph**) showing a molecular junction sustain (light color) or rupture (dark color) under a 0.9 V applied bias. Dashed vertical lines show the range of the molecular junction's conductance as determined from the conductance histograms in Figure 1. Inset shows the breaking probability as a function of the applied peak voltage for **Si2** (**Si2Naph**) and the error bars show the standard deviation determined from variations in sets of thousand measurements.

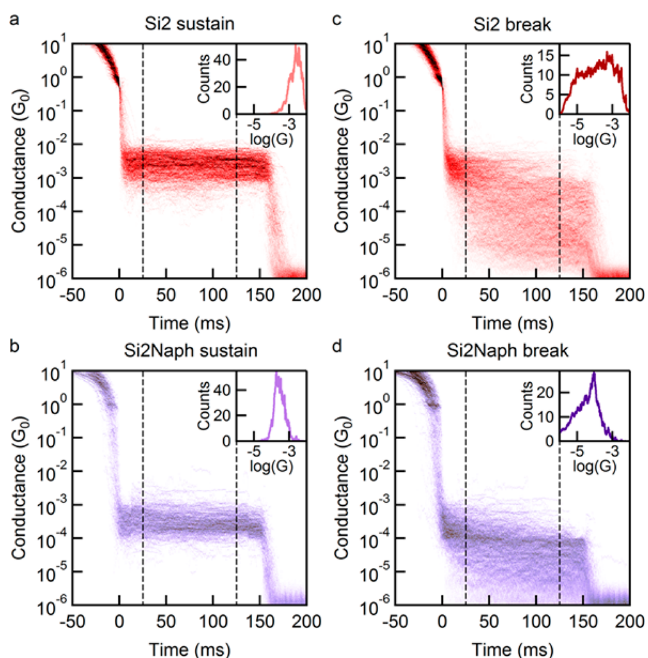

Figure 3. Two-dimensional conductance histograms of all traces showing sustaining junctions of (a) **Si2** and (b) **Si2Naph** and breaking junctions of (c) **Si2** and (d) **Si2Naph** while a voltage of 0.9 V is applied during the time indicated by the region in between the two dashed lines. Each inset shows a conductance distribution of its corresponding 2D histogram while the high bias is applied.

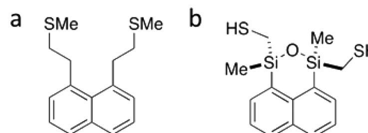

Figure 4. Chemical structures of (a) 1,8-bis(2-(methylthio)ethyl)-naphthalene and (b) siloxane **5**.

from Figure 1c). For the junctions that rupture, we find that the distribution of the conductance for **Si2** is across a wide range 10^{-2}–10^{-6} G_0, whereas the conductance for **Si2Naph** shows a distribution that is sharply peaked at 10^{-4} G_0.

We hypothesize that the Si–Si bond can rupture under an applied bias of 0.9 V in both cases: **Si2Naph** can still conduct through the 1,8-substituted naphthalene system but **Si2** has no conduction pathway when Si–Si bond is broken. This explains the clear conductance observed for junctions with **Si2Naph** when the Si–Si bond is broken, which is not observed in the broken **Si2** junction. To show that the **Si2Naph** can conduct through the 1,8-connection across the naphthyl bridge, we synthesize 1,8-bis(2-(methylthio)ethyl)naphthalene (structure in Figure 4a), measure its conductance, and find a clear conductance signature (conductance histogram in SI Figure S2). This result shows that 1,8 substituted naphthalene bridging the Au electrodes can provide electron transport pathways, likely through the sigma system as the π-system should evidence a destructive quantum interference effect.[18]

One possible mechanism for the Si–Si bond rupture in the **Si2Naph** system could involve an oxidative addition of the Au to the bond, and we note that oxidative addition of Au nanoparticles to Si–Si bonds has been demonstrated.[19,20] However, and in contrast to our recent study,[15] we do not see any evidence for a contact between the Au electrodes and the Si–Si bond in the conductance histograms. Further, we have observed no evidence for the formation of an alternative molecular junction upon rupture of the Si–Si bond, or the reformation of the junction. We suggest that rotation about one or both of the naphthyl—Si bonds subsequent to Si–Si cleavage could prevent bond reformation.

Another possibility we considered is high-bias induced oxidation of the disilane to the siloxane because these experiments are performed under ambient conditions.[19] To test this hypothesis, we independently synthesize the siloxane[21] corresponding to **5** (structure in Figure 4b). We find that its conductance is 1.5 times the conductance of the broken **Si2Naph** junction (conductance histogram in SI Figure S3). We conclude that it is unlikely that the conductance we observe upon Si–Si bond rupture may be attributed to the formation of the siloxane.

Density Functional Theory Calculations. We now turn to ab initio computations carried out using density functional theory and molecular dynamics to understand the mechanism of the voltage-induced bond rupture processes observed here. We first consider impact of an applied voltage on the junction to see if any Stark effect[22] could polarize the Si–Si bond, thus destabilizing it. We construct a molecular junction using electrodes that consist of seven layers of 16 gold atoms on both sides terminated by a trimer that serves as a tip structure on which the molecule is bound. This junction is relaxed using

DOI: 10.1021/jacs.6b10700
J. Am. Chem. Soc. 2016, 138, 16159–16164

DFT within the GGA of Perdew, Burke, and Ernzenhof (PBE)[23,24] and a double-ζ-basis set as implemented in SIESTA.[25,26] Details of our DFT calculations are provided in a previous work.[27] The DFT optimized junction geometry is first determined and then a bias-dependent steady-state density matrix is calculated self-consistently following a standard first-principles approach.[28,29] A bias voltage of 1.0 V is applied to the junction by fixing the chemical potential of the two electrodes symmetrically around the junction Fermi level and the potential profile across the molecule is obtained. From this profile, we find that about 15% of the voltage drops across the Si−Si bond in the Au−**Si2Naph**−Au junction (SI Figure S4). This indicates that with a bias of 1.0 V applied on the junction, the Si−Si bond is under a 0.09 V/Å electric field, which is unlikely to have any significant impact on the bond.[30−32] We add further that transmission calculations for similar junctions have shown that there are no molecular resonances accessible within the bias window and thus transport is through an off-resonance tunneling mechanism.[33]

We therefore conclude that bond rupture is through a current-induced mechanism where the incoming electrons excite molecular vibrational modes of the junction. We calculate the vibrational modes of **Si2** and **Si2Naph** both in the isolated case and as a junction using DFT with a finite difference procedure. The dynamical matrix is generated using displacements of 0.025 Å for each atom, along each Cartesian direction. In the case of the junction, forces are computed using four layers of gold on each side, with only the topmost layer and the binding motif included in the dynamical matrix, corresponding to 384 and 432 displacements for the **Si2** and **Si2Naph** junctions, respectively.

In Figure 5, we plot the calculated vibrational spectra for **Si2** (red) and **Si2Naph** (purple) with the tick marks showing the decomposition of the Si−Si stretch modes with significant displacement (for details, see SI Figures S5−S8). For **Si2**, the Si−Si stretch is maximal for the modes at 28.9 and 50.8 meV, with non-negligible displacements for up to 103 meV. For **Si2Naph**, there is significant hybridization of the Si−Si stretch and the Si−Naphthalene stretch, leading to a denser spectrum of modes with significant Si−Si stretch in the 28−60 meV energy range. We first note that there are many Si−Si vibrational modes at low energies that can be relatively easily excited as long as the voltage across the junction is greater than ~200 mV. We note further that, due to their heavy mass, the Au-related modes are all at energies below 20 meV, i.e., spectrally decoupled from the Si−Si stretch modes. Finally, we find that a mode around 320 meV, which corresponds to an S−H stretching mode is shifted to low energies upon the formation of an S−Au bond and H desorption.

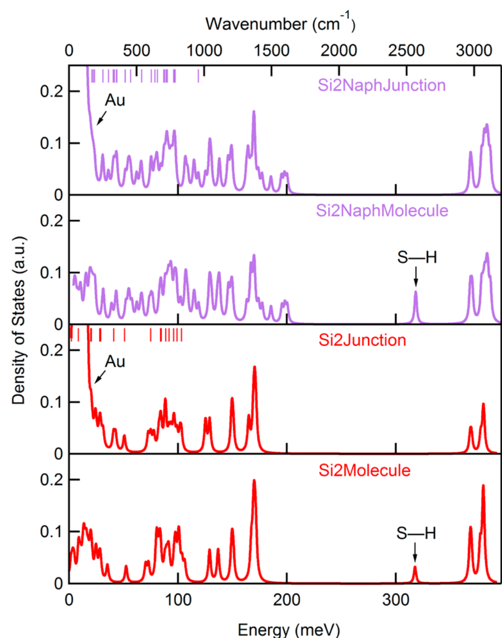

Figure 5. Calculated vibrational modes for **Si2** (red) and **Si2Naph** (purple) for the molecule and molecular junction (including the electrodes) configurations. The vertical tick marks indicate the decomposition of the most significant Si−Si stretch modes.

We have also calculated the vibrational spectra of **Si2** and **Si2Naph** at finite electric fields (−1 ~ +1 V) and do not see any strong field-dependence (SI Figure S9, S10) or any charging dependence (SI Figure S11, S12) in agreement with the weak voltage drop found at the Si−Si bond (SI Figure S4).[34] We conclude that we can excite the Si−Si modes at all biases where we observe bond rupture. As the voltage is increased, the probability that these vibrational modes are excited increases as the composition of the scattering states around the Fermi energy has a weak energy dependence, and wider bias windows enable multiple excitations to the vibrational modes. This proposed mechanism indicates that the Si−Si bond rupture is a simple, direct homolytic cleavage as opposed to heterolysis or disintegration.

Molecular Dynamics Simulations. Next, we carry out ab initio molecular dynamics (MD) simulations of bond stability at different finite temperatures using an NVT ensemble and the SIESTA code.[26] We model the junctions with one fixed layer of gold on each side and an adatom binding motif (SI Figure S13). We compute 5 ps-long MD trajectories using a 1 fs time step at constant volume and temperature. We compute the pair-distribution function for temperatures ranging from 300 to 1600 K and determine the length of the Si−Si, Si−C, and Au−S bonds at each temperature. In Figure 6, we plot the length distributions for these bonds in a **Si2** molecular junction at different temperatures. We see that at temperature above ~1000 K, the Si−Si bond length varies by as much as 20% from the energy minimum bond length while the Au−S bond length distributions show only a modest increase, and the C−Si bond length distributions do not show any significant increase. Although these temperatures are in excess of the local temperature in molecular devices,[35] they are compatible with nonequilibrium mode occupations induced by large current densities in a slowly thermalizing environment.[36] This indicates that if the molecular vibrational modes are indeed excited by the current, the Si−Si bond is most likely to rupture.

CONCLUSIONS

To conclude, we demonstrate an experimental method to investigate the bond stability under an electric field using single molecule circuits. In this study, we apply this method to **Si2** and **Si2Naph** single molecule junctions and find different transport properties between them when the junctions rupture under an electric field. This provides strong evidence that a Si−Si bond ruptures in both cases. We further investigate the bond rupture mechanism through density functional theory and molecular dynamics calculations and conclude that excitation of the vibrational modes in the molecular junction is the cause of bond rupture in our measurements. The studies described here

DOI: 10.1021/jacs.6b10700
J. Am. Chem. Soc. 2016, 138, 16159−16164

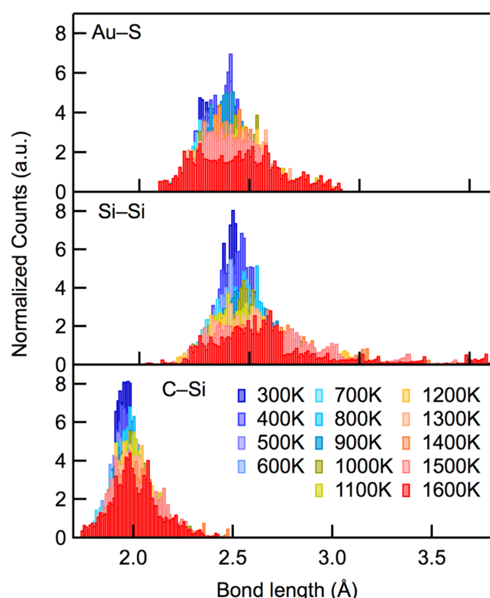

Figure 6. Molecular dynamics simulations showing distributions of bond lengths for Si–Si (top), Si–C (middle), and Au–S (bottom) bonds as a function of temperature in a **Si2** molecular junction. Color scale indicates temperature range of 300–1600 K or 25.8–137.9 meV.

help deepen our understanding of the nature of the chemical bond in extreme environments.

■ ASSOCIATED CONTENT

Supporting Information

The Supporting Information is available free of charge on the ACS Publications website at DOI: 10.1021/jacs.6b10700.

Additional data, characterizations and methods (PDF)

■ AUTHOR INFORMATION

Corresponding Authors

*M.L.S. mls2064@columbia.edu
*C.N. cn37@columbia.edu
*P.D. pdarancet@anl.gov
*J.L.L. leighton@chem.columbia.edu
*L.V. lv2117@columbia.edu

ORCID

Haixing Li: 0000-0002-1383-4907
Colin Nuckolls: 0000-0002-0384-5493
Latha Venkataraman: 0000-0002-6957-6089

Present Address

T.A.S.: Department of Chemistry, University of California, Berkeley, Berkeley, CA 94720, United States

Notes

The authors declare no competing financial interest.

■ ACKNOWLEDGMENTS

We thank the National Science Foundation for the primary support of this work under Grant CHE-1404922. H.L. is supported in part by the Semiconductor Research Corporation and New York Center for Advanced Interconnect Science and Technology Program. Use of the Center for Nanoscale Materials, an Office of Science user facility, was supported by the U.S. Department of Energy, Office of Science, Office of Basic Energy Sciences, under Contract No. DE-AC02-06CH11357. P.D. thanks Badri Narayanan for helpful discussions.

■ REFERENCES

(1) Tao, L.; Cinquanta, E.; Chiappe, D.; Grazianetti, C.; Fanciulli, M.; Dubey, M.; Molle, A.; Akinwande, D. *Nat. Nanotechnol.* **2015**, *10* (3), 227–231.
(2) Colinge, J.-P.; Lee, C.-W.; Afzalian, A.; Akhavan, N. D.; Yan, R.; Ferain, I.; Razavi, P.; O'Neill, B.; Blake, A.; White, M.; Kelleher, A.-M.; McCarthy, B.; Murphy, R. *Nat. Nanotechnol.* **2010**, *5* (3), 225–229.
(3) Shen, X.; Sun, B.; Liu, D.; Lee, S.-T. *J. Am. Chem. Soc.* **2011**, *133* (48), 19408–19415.
(4) Tian, B.; Zheng, X.; Kempa, T. J.; Fang, Y.; Yu, N.; Yu, G.; Huang, J.; Lieber, C. M. *Nature* **2007**, *449* (7164), 885–889.
(5) Yu, P.; Tsai, C.-Y.; Chang, J.-K.; Lai, C.-C.; Chen, P.-H.; Lai, Y.-C.; Tsai, P.-T.; Li, M.-C.; Pan, H.-T.; Huang, Y.-Y.; Wu, C.-I.; Chueh, Y.-L.; Chen, S.-W.; Du, C.-H.; Horng, S.-F.; Meng, H.-F. *ACS Nano* **2013**, *7* (12), 10780–10787.
(6) Shin, H.; Qiu, W.; Jarecki, R.; Cox, J. A.; Olsson, R. H.; Starbuck, A.; Wang, Z.; Rakich, P. T. *Nat. Commun.* **2013**, *4*, 1944.
(7) Van Laer, R.; Kuyken, B.; Van Thourhout, D.; Baets, R. *Nat. Photonics* **2015**, *9* (3), 199–203.
(8) Löfås, H.; Orthaber, A.; Jahn, B. O.; Rouf, A. M.; Grigoriev, A.; Ott, S.; Ahuja, R.; Ottosson, H. *J. Phys. Chem. C* **2013**, *117* (21), 10909–10918.
(9) Su, T. A.; Li, H.; Steigerwald, M. L.; Venkataraman, L.; Nuckolls, C. *Nat. Chem.* **2015**, *7* (3), 215–220.
(10) Sanderson, R. T. *J. Am. Chem. Soc.* **1983**, *105* (8), 2259–2261.
(11) Li, H.; Su, T. A.; Zhang, V.; Steigerwald, M. L.; Nuckolls, C.; Venkataraman, L. *J. Am. Chem. Soc.* **2015**, *137* (15), 5028–33.
(12) Kiely, J. S.; Boudjouk, P. *J. Organomet. Chem.* **1979**, *182* (2), 173–183.
(13) Ando, W.; Wakahara, T.; Akasaka, T.; Nagase, S. *Organometallics* **1994**, *13* (12), 4683–4685.
(14) Wakahara, T.; Kodama, R.; Akasaka, T.; Ando, W. *Bull. Chem. Soc. Jpn.* **1997**, *70* (3), 665–670.
(15) Kim, N. T.; Li, H.; Venkataraman, L.; Leighton, J. L. *J. Am. Chem. Soc.* **2016**, *138* (36), 11505–11508.
(16) Xu, B.; Tao, N. J. *Science* **2003**, *301* (5637), 1221.
(17) Venkataraman, L.; Klare, J. E.; Tam, I. W.; Nuckolls, C.; Hybertsen, M. S.; Steigerwald, M. L. *Nano Lett.* **2006**, *6* (3), 458–462.
(18) Solomon, G. C.; Andrews, D. Q.; Hansen, T.; Goldsmith, R. H.; Wasielewski, M. R.; Van Duyne, R. P.; Ratner, M. A. *J. Chem. Phys.* **2008**, *129* (5), 054701.
(19) Gryparis, C.; Kidonakis, M.; Stratakis, M. *Org. Lett.* **2013**, *15* (23), 6038–6041.
(20) Gryparis, C.; Stratakis, M. *Chem. Commun. (Cambridge, U. K.)* **2012**, *48* (87), 10751–3.
(21) Klausen, R. S.; Widawsky, J. R.; Steigerwald, M. L.; Venkataraman, L.; Nuckolls, C. *J. Am. Chem. Soc.* **2012**, *134* (10), 4541–4.
(22) Hochstrasser, R. M. *Acc. Chem. Res.* **1973**, *6* (8), 263–269.
(23) Perdew, J. P.; Burke, K.; Ernzerhof, M. *Phys. Rev. Lett.* **1996**, *77* (18), 3865–3868.
(24) Perdew, J. P.; Burke, K.; Ernzerhof, M. *Phys. Rev. Lett.* **1997**, *78* (7), 1396–1396.
(25) Ordejón, P.; Artacho, E.; Soler, J. M. *Phys. Rev. B: Condens. Matter Mater. Phys.* **1996**, *53* (16), R10441–R10444.
(26) Soler, J. M.; Artacho, E.; Gale, J. D.; García, A.; Junquera, J.; Ordejón, P.; Sánchez-Portal, D. *J. Phys.: Condens. Matter* **2002**, *14* (11), 2745.
(27) Darancet, P.; Widawsky, J. R.; Choi, H. J.; Venkataraman, L.; Neaton, J. B. *Nano Lett.* **2012**, *12* (12), 6250–6254.
(28) Choi, H. J.; Cohen, M. L.; Louie, S. G. *Phys. Rev. B: Condens. Matter Mater. Phys.* **2007**, *76* (15), 155420.
(29) Brandbyge, M.; Mozos, J.-L.; Ordejón, P.; Taylor, J.; Stokbro, K. *Phys. Rev. B: Condens. Matter Mater. Phys.* **2002**, *65* (16), 165401.
(30) Lou, L.; Nordlander, P. *Phys. Rev. B: Condens. Matter Mater. Phys.* **1996**, *54* (23), 16659–16662.

(31) Choi, Y. C.; Pak, C.; Kim, K. S. *J. Chem. Phys.* **2006**, *124* (9), 094308.
(32) Vegiri, A.; Schevkunov, S. V. *J. Chem. Phys.* **2001**, *115* (9), 4175−4185.
(33) Li, H.; Garner, M. H.; Shangguan, Z.; Zheng, Q.; Su, T. A.; Neupane, M.; Li, P.; Velian, A.; Steigerwald, M. L.; Xiao, S.; Nuckolls, C.; Solomon, G. C.; Venkataraman, L. *Chem. Sci.* **2016**, *7* (9), 5657−5662.
(34) Li, Y.; Doak, P.; Kronik, L.; Neaton, J. B.; Natelson, D. *Proc. Natl. Acad. Sci. U. S. A.* **2014**, *111* (4), 1282−1287.
(35) Huang, Z.; Chen, F.; D'Agosta, R.; Bennett, P. A.; Di Ventra, M.; Tao, N. *Nat. Nanotechnol.* **2007**, *2* (11), 698−703.
(36) Chen, Y.-C.; Zwolak, M.; Di Ventra, M. *Nano Lett.* **2003**, *3* (12), 1691−1694.

DOI: 10.1021/jacs.6b10700
J. Am. Chem. Soc. 2016, 138, 16159−16164